Spatial modeling of deep-sea ferromanganese nodules with limited data using neural networks

Vishnu N. Hari, *Member, IEEE*, Bharath Kalyan, *Member, IEEE*, Mandar Chitre, *Senior Member, IEEE*, Varadarajan Ganesan
Keppel-NUS Corplab and Acoustic Research Laboratory,
National University of Singapore

***Abstract*—Deep-sea ferromanganese nodules found in the Clarion-Clipperton zone (CCZ) in the Pacific ocean are a large potential source of metals such as nickel, cobalt and manganese. Spatial modeling of these nodules is essential to obtain a better scientific understanding about their formation and distribution, and conduct feasibility studies on their exploitation. However, data on the quantitative and qualitative distribution of nodules in CCZ are sparse and often not divulged, and the accuracy of conventional spatial modeling techniques is limited by this scarcity of data. We present an approach based on artificial neural networks for modeling nodule parameters in the CCZ using the limited data available in the open domain. Our model's predictions are comparable to benchmark predictions from the International Seabed Authority which used a more extensive data set. Moreover, our model can predict small as well as large-scale variations of nodules, which are essential in making evaluations for deep-sea harvesting. We discuss the contribution of each factor in the modeling, and show that small-scale nodule parameter variations can be effectively predicted by incorporating the local topography.**

***Index Terms*—manganese nodules, Clarion-Clipperton zone, neural network, spatial model, deep sea**

I. INTRODUCTION

A. Ferromanganese nodules

FERROMANGANESE (FMN) nodules are potato-sized concretions containing metals such as iron, manganese, nickel and cobalt. They are found in several regions in the world's oceans and have been identified as a resource of nickel, cobalt, manganese, lead, lithium, and rare earth metals [1]–[6]. In the light of diminishing land-based resources, deep-sea FMN deposits hold the potential to become the main source for these metals in the future, especially nickel and cobalt [1], [4], [7]. Over the last few decades, the exploitation of nodules has been increasingly considered in terms of its commercial feasibility, political factors and environmental impacts [4], [8]–[11]. One of the geographical areas in focus for the exploration of these resources is the Clarion-Clipperton zone (CCZ) in the north Pacific.

B. Modeling: review, aims and challenges

The CCZ covers roughly 12.57 million square kilometers [12]. It has been rigorously explored through a series of cruises, yet the total data available on the area is sparse. It is not feasible to survey this area in a short amount of time given the hefty costs involved in conducting exploratory cruises. In this scenario, the ideal strategy to obtain a preliminary estimate of resources is spatial modeling.

Spatial modeling broadly refers to describing the spatial variation of resources in terms of parameters such as their abundance, quality and usability. It is of immense interest for the study, exploration or exploitation of resources. It can give predictions on where resources are likely to be found and how economically they can be mined, which is significant from a commercial perspective. A good spatial prediction model reduces the time and money spent on finding suitable harvesting sites. From a scientific perspective, it helps us understand the mechanism of formation and distribution of these resources. In the context of FMN exploration in the CCZ, spatial modeling is vital to bridge the gap between:

- our understanding of the genesis of FMN and factors affecting their abundance and quality,
- making useful predictions on where to find them, and to strategize and plan for exploration/harvesting missions, and
- making estimates that are crucial in deciding their exploitation and commercial feasibility.

Spatial modeling of FMN has been undertaken previously by many, having been identified as an important research area [11], [13]–[18]. Frazer and Fisk give a detailed review of the related literature prior to the 1980s [15]. Cronan discussed a set of control factors affecting nodule genesis [19]. Kim et al. presented studies on the area allocated to South Korea in the CCZ [17]. McKenzie et al. have undertaken weights-of-evidence modeling of nodules in the Cook Islands Exclusive Economic zone (CIEZ) [18]. In 2003, the International Seabed Authority (ISA) convened a workshop to discuss the geological modeling of FMN deposits in CCZ to aid resource assessments. Subsequently, suitable proxy variables were determined and some geological models were developed and summarized in an ISA technical report [12] which consisted of two sub-reports [20], [21].

The CCZ has been unevenly explored, and all the surveys together constitute only a small fraction of the CCZ area. This data scarcity limits the effectiveness of interpolated models and methods like kriging which rely on spatial correlation of FMN deposits across the CCZ to make predictions. A more reliable approach would be to build a model that uses surrogate variables and principles related to the genesis of these nodules. We can then train the model to be an effective predictor even in regions where prior data on FMN deposits is unavailable, as long as we use sufficient surrogate parameter data. This is because the principles of formation of FMN must hold true even in such regions. Thus, a good spatial modeling strategy for the CCZ would be to efficiently use the limited FMN data available to develop a model applicable in all regions of interest.

Commercial players in FMN exploration are often reluctant to share data on FMN and related surrogate variables. This limitation on data availability makes it challenging for new parties to develop spatial models and make first-order resource estimates of their areas. The other challenge is of scale. Use of surrogate parameters such as net primary productivity (NPP) can explain large-scale variations [15], [19]. However, to explain small-scale variations of FMN, one must use other factors such as local topography and sediment-type [15]. Developing a model that can generalize both large and small-scale variations involves blending the effects of all these factors together in an efficient way.

The following is a summary of our contributions:

- We outline a methodology of spatial modeling of FMN in the CCZ using the limited amount of data available in the open domain. This includes surrogate data consisting of bathymetry, NPP and geophysical data, and data on nodule density, nodule presence and percentage (%) of elements in the nodules.
- Ours is not a bio-geo-chemical model, but rather a data-driven one that models variations in the data aided by our understanding of nodule formation.
- The modeling is based on artificial neural networks (ANN), which are effective in modeling unknown underlying variations in the data [22].
- In order to model the small-scale variations, we use features representing the geophysical data and the local topography extracted from bathymetric data.
- We show that with efficient modeling techniques and smart use of data, it is possible to model the FMN variation well despite limitations on the amount of data available.
- Our model consistently outperforms conventional interpolation approaches of predicting nodule parameters for unknown locations.
- We benchmark our model against the predictions in the report by ISA [12].

The paper is organized as follows. So far, we have covered the aims, challenges and review of FMN and their spatial modeling. In section II, we review the literature on the mechanism and factors responsible for nodule formation. We then describe the selection and processing of open-domain data relevant to our modeling method in sections III and IV. Here we outline the surrogate factors used and the nodule parameters modeled in this paper. In section V, we present the methodology of modeling the nodule variations using ANNs. Finally, in section VI, we discuss the results of the modeling, and conclude the paper in section VII. Henceforth, we will use the chemical symbols representing elements such as manganese (Mn), iron (Fe), nickel (Ni), cobalt (Co), copper (Cu), Lithium (Li) and zinc (Zn) throughout the paper for brevity.

TABLE I
NUMBER OF DATA POINTS OBTAINED AND OPEN-DOMAIN SOURCES ON NODULE PARAMETERS

Nodule parameter	No. of points
Nodule density (kg/m^2)	454
Nodule presence	1622
Ni %	572
Co %	509

II. Mechanism and factors affecting nodule formation

A. Mechanism

FMN are formed by accretion of oxides of metals like Mn, Fe, Ni, Co, Cu, and rare-earth metals in deep-sea regions [14]. The primary sources of these metals to the oceans are terrigenous, volcanogenic and atmospheric [12]. The metal particles from these sources are ingested by plankton in the photic zone and sink to the ocean bottom as fecal pellets. At the bottom, nodules are formed by concentration of these metals via a combination of diagenetic and hydrogenetic processes [23].

Diagenesis refers to the entry of metals like Ni, Cu and Zn into the nodules from pore waters, whereas hydrogenesis refers to the entry of metals like Fe and Co directly from the seawater [23]. In both processes, the presence of a nucleus is necessary for nodule formation [24]. The ratio of hydrogenesis to diagenesis is a key factor that determines the variation of nodule properties that are of commercial significance. The dominance of diagenesis leads to higher concentrations of Ni, Cu and Zn, and higher Mn-to-Fe ratio. Areas with greater hydrogenesis generally yield nodule deposits with greater abundance and higher Co % in their weight. Consequently, factors associated with diagenetic formation such as Mn-to-Fe ratio, Cu%, Ni% and overall nodule grade, are negatively correlated with nodule density [15], [25], which Healing and Archer likened to a Lasky distribution [13].

B. Factors

Proximity to the source of metals is one obvious factor that influences nodule formation. Terrigenous sources such as continental run-off from the western coast of north America (WCA) contribute most of the Ni and Cu content in FMN, and contribute Mn to a smaller degree. Volcanogenic content consists of metals injected into the ocean from hydrothermal vents along the east Pacific rise (EPR), and are the main source for Co and Mn [37]. Some geological studies suggest that volcanic activity along the Mahi-Mahi Fracture zone (MMFZ) may also have contributed metal content for nodule formation [12], but this mention is lacking in other literature. This could be because the MMFZ is considered about 30 to 40 million years old, which is older than the period when nodule formation started.

From an inspection of the nodule density data collected by us, we observe a general decrease in nodule density from east

TABLE II
OPEN-DOMAIN SOURCES OF DATA ON FACTORS

Factor	Sources
Bathymetry	General bathymetric grid of the ocean [26], [27], Online databases at NCEI [28]
Sediment-type	Online databases at NCEI [28], primarily the Seadas database, consisting of the following: The NOAA and MMS Marine Minerals Bibliography [29], Archive of Core and Site/Hole Data and Photographs from the Ocean Drilling Program (ODP) [30], NOAA/NOS and USCGS Seabed Descriptions from Hydrographic Surveys [31], Index to Marine and Lacustrine Geological Samples (IMLGS) [32], Archive of Core and Site/Hole Data and Photographs from the Integrated Ocean Drilling Program (IODP) [33], Archive of Core and Site/Hole Data and Photographs from the Deep Sea Drilling Project (DSDP) [34] and ISA Central Data Repository [35]
NPP (mg·C/(m^2·day))	Oregon State University [36]
Distance from EPR, MMFZ and WCA	Computed based on locations obtained from ISA report [12]

to west in the CCZ. This can also be observed in the maps provided by ISA [12] and is corroborated by Morgan [38] who mentions that highest nodule-density areas are found in the east. The belt of highest nodule density is located halfway between the Clarion and Clipperton Fracture zones [38]. This distribution seems to be correlated to the distance from the EPR and MMFZ.

The concentration of metals like Ni and Cu also depends on the biological activity on the sea surface which determines the flux of these metals to the ocean floor [19]. A direct indicator which reflects the biological photosynthetic activity is NPP, which is the flux rate of carbon in surface plankton [39]. The surface chlorophyll content (SCC), which indicates the amount of chlorophyll of surface plankton, is used as a proxy variable for NPP in the ISA report [12].

Another factor that determines nodule formation at a location is its depth relative to the carbon compensation depth (CCD) [19]. The CCD is the depth within the ocean water column at which the dissolution of calcium carbonate is balanced by its sedimentation rate. If the seafloor lies above the CCD, nodule formation will be inhibited by dilution from precipitating carbonates; below the CCD, this will not be the case [19].

Local topography and sedimentation rate are key parameters determining small-scale variations in nodule parameters. This has been corroborated by studies throughout the world [40], [41]. Usui et al. [14] and Sharma et al. [16] suggest that diagenesis dominates in areas with high sedimentation rates, and hydrogenesis dominates in areas with low sedimentation rates. A study in the Korea Deep Ocean Study area also notes that hydrogenesis is most common where local topography is rugged and sedimentation rates are low, while diagenesis is common in abyssal plains where sedimentation rates are high [12], [17]. Studies from the CCZ [42], central Pacific [14] and Indian ocean [16] note that high sedimentation impedes nodule formation due to two possible reasons. Firstly, high sedimentation impedes the bioturbation which provides a lifting force necessary for nodule formation [14]. Secondly, it creates a blanket cover over the region, preventing exposure of sufficient nuclei for nodule formation such as fragmented rocks [16].

Low sedimentation is correlated with areas of undulating topography and high bottom-water current [12], [17], [41]. Consequently, areas of high topographic variation and current are favorable for nodule formation. Though most authors agree that sedimentation rates depend on the bottom-water currents [15], [17], Mewes et al. describe a more complex relationship of the currents and sedimentation rates on the local topography [41]. Currents may generate more nuclei through erosion, leading to an increase in nodule formation. The presence of currents also impedes sedimentation, which is beneficial for nodule formation.

Frazer and Fisk noted that topography accounts for the largest variation in nodule element ratios, and that variation of Co content in nodules was highly correlated with the depth [15]. Sharma et al. state that high nodule density is generally observed near hills near the sides or at the bottom, where the hydrogenetic process dominates [16]. Interestingly, this region is also highly amenable to the formation of Co-rich Mn crusts.

The sediment-type is described as an effective factor in predicting nodule parameters [12], [15]. It reflects the depth in relation to the CCD, the sedimentation rates, and the kind of biological activity in the sediment. The sediment can be categorized as siliceous, calcareous or pelagic clay. Generally, siliceous sediments are observed to be the most favorable for nodule formation, followed by pelagic clay, whereas calcareous sediments are less favorable. This is correlated to the observation that nodules are abundant in regions below the CCD.

III. FACTORS SELECTED FOR MODELING

The factors we select based on our discussions in section II include the NPP, for which data is available online, and distances from the EPR, MMFZ and WCA which can be computed based on the locations of these features. But modeling based on these factors is effective only in explaining large-scale variations. Small-scale variations are better explained by local topography and sediment-type factors. We are unable to use CCD and benthic currents as factors because data on them are not easy to obtain.

To summarize, we consider bathymetry, local topography, sediment-type, NPP and distance from the WCA, EPR and MMFZ as factors. We outline our approach to the use of these factors in the following subsections.

A. Bathymetry and Local topography

All previous attempts to model the effects of topography followed the approach of classifying topographic features into

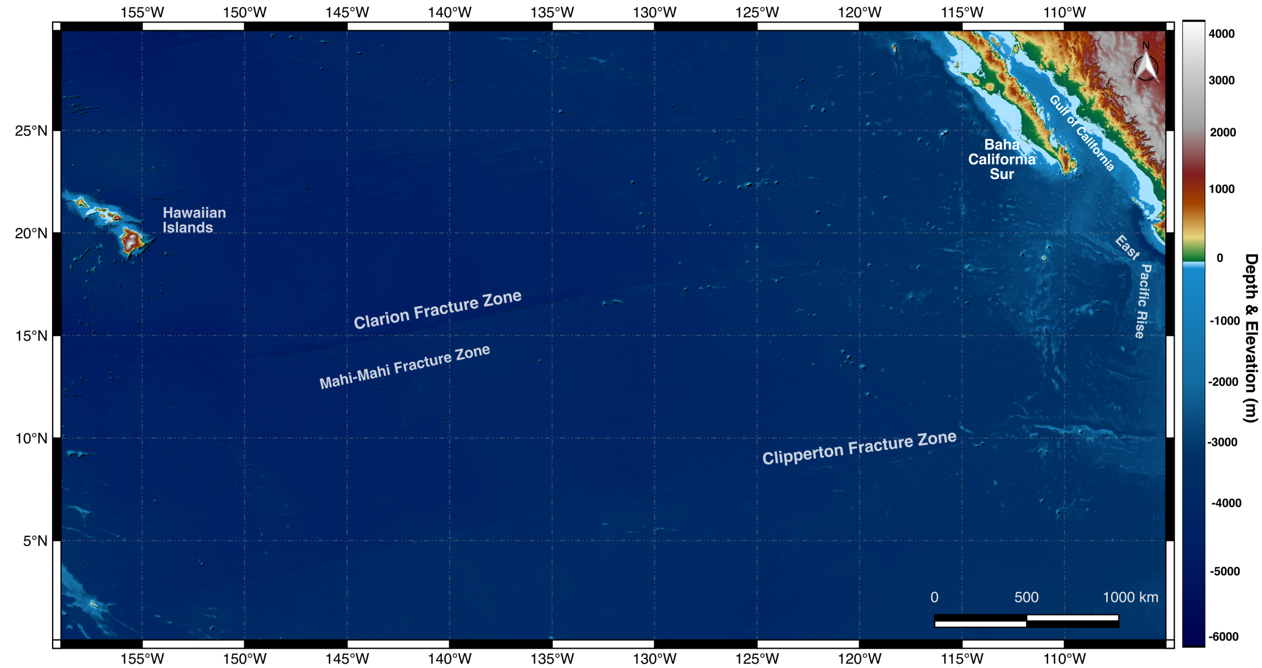

Fig. 1. Bathymetric map indicating the CCZ and other geographical features used in modeling, in the northeast Pacific.

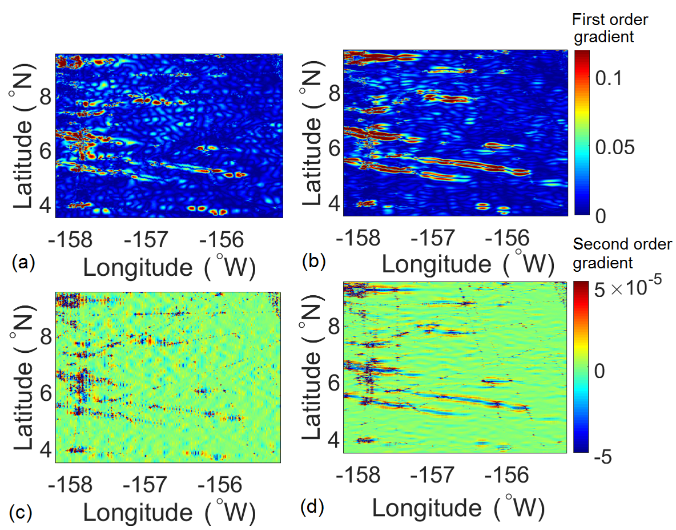

Fig. 2. Magnified map of topographic factors within region bounded by 155° W to 158° W, and 3.5° N to 9° N, showing small-scale features: (a) Δ_x^1, (b) Δ_y^1, (c) Δ_x^2, (d) Δ_y^2.

categories like abyssal seamounts, ridges and plains. This approach relies on classifications hand-picked by the modeler, and does not quantify the variation in topography. Thus, the performance is heavily reliant on the effectiveness of the manual classification. Automatic classification of topographic features is a non-trivial pattern classification problem out of the scope of this paper. Moreover, by relying on these feature categories during modeling, we lose some finer underlying details such as the magnitude of the topographic variation.

A novel approach we use in our modeling is to quantify the topographic variation in terms of numerical quantities, namely, the depth and the directional depth gradients at each point. The gradients can help us distinguish the local topography at a location and broadly identify whether it refers to a hill, valley, plain, etc. Thus, it can be used in ANNs to incorporate the dependence on local topography. Models learnt based on these quantities can be interpreted in terms of corresponding topographic variations. Additionally, this allows the ANN model to learn details that depend on the magnitude of the variation, which is captured in the quantification of the topographic features.

We compute the gradients as follows. Assume that the bathymetry is available as a function of latitude and longitude as $d(a,b)$, where a denotes the latitude and b denotes the longitude. Also, denote the horizontal distance between two points at lat-long coordinates (a_1,b_1) and (a_2,b_2) as $H(a_1,b_1,a_2,b_2)$. For any point with latitude a and longitude b, we compute

- First-order depth gradient in eastward direction

$$\Delta_x^1(a,b,\epsilon) = \frac{d(a,b+\epsilon) - d(a,b-\epsilon)}{H(a,b+\epsilon,a,b-\epsilon)}, \quad (1)$$

- Second-order depth gradient in eastward direction

$$\Delta_x^2(a,b,\epsilon) = \frac{\Delta_x^1(a,b+\frac{\epsilon}{2},\frac{\epsilon}{2}) - \Delta_x^1(a,b-\frac{\epsilon}{2},\frac{\epsilon}{2})}{H(a,b+\epsilon,a,b-\epsilon)}, \quad (2)$$

- First-order depth gradient in northward direction

$$\Delta_y^1(a,b,\epsilon) = \frac{d(a+\epsilon,b) - d(a-\epsilon,b)}{H(a+\epsilon,b,a-\epsilon,b)}, \quad (3)$$

- Second-order depth gradient in northward direction

$$\Delta_y^2(a,b,\epsilon) = \frac{\Delta_y^1(a+\frac{\epsilon}{2},b,\frac{\epsilon}{2}) - \Delta_y^1(a-\frac{\epsilon}{2},b,\frac{\epsilon}{2})}{H(a+\epsilon,b,a-\epsilon,b)}, \quad (4)$$

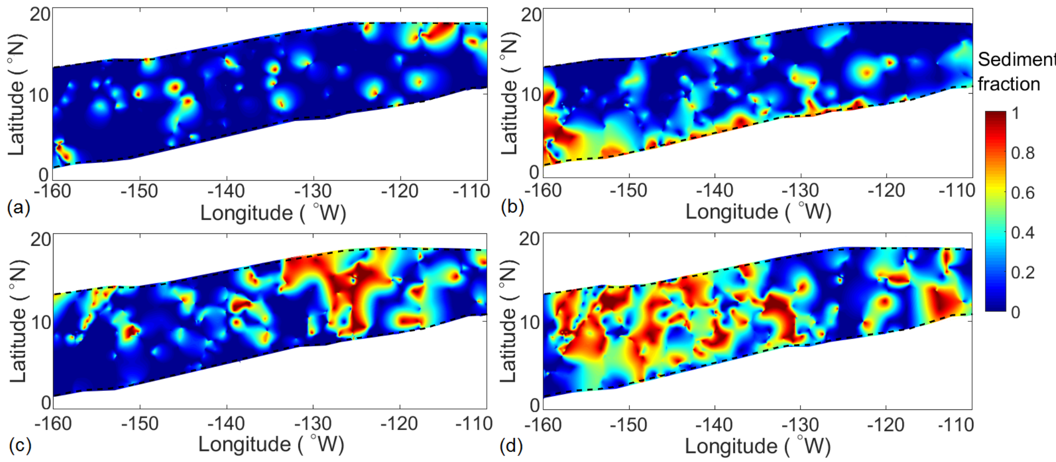

Fig. 3. Variation of sediment-type fractions of (a) terrigenous material S_t, (b) calcareous sediment S_c, (c) pelagic clay S_p, (d) siliceous sediment S_s over the CCZ

where ϵ is the lat-long resolution around the point (a, b) chosen for gradient computation.

A bathymetric map of the northeast Pacific showing the CCZ, is plotted in Fig. 1. The map indicates the Clarion and Clipperton fracture zones between which lies the CCZ. The depth gradients are computed based on the bathymetric information. In Fig. 2, we plot the depth gradients computed for a small region bounded by $155°$ W to $158°$ W, $3.5°$ N to $9°$ N, to depict the small-scale variations captured by the gradients.

B. Sediment-type

A limited amount of low-resolution data on sediment-type in CCZ is available on some online repositories. We interpolate the information from these sources for regions where this data is unavailable. Based on the data, we characterize the sediment-type in terms of fractions of four categories of content that the sediment contains:

1) Terrigenous material of large size (rocks, sand, silt) with little or no biological content
2) Pelagic clay
3) Siliceous sediment
4) Calcareous sediment

Previous models used sediment-type as a factor by categorizing the data into siliceous, pelagic and calcareous sediments as part of pre-processing. Our approach allows us to train the ANN using the quantified fraction values, rather than using a rigid categorical classification. This removes the dependence of modeling performance on the classifications hand-picked by the modeler. It also opens up the possibility of spotting new trends like the effect of siliceous-calcareous oozes or that of the biogenous content in the sediment.

For each location, the fractions of content are denoted by S_t, S_p, S_s and S_c for terrigenous, pelagic clay, siliceous and calcareous type of sediments respectively. We assume that the sediment at any place can be fully characterized by these four types of content. Hence $S_s + S_t + S_p + S_c = 1$. In Fig. 3, we plot a map of sediment-type fractions interpolated over the whole of CCZ based on the data we collected. In this map and all the maps presented henceforth, the Clarion and Clipperton fractures will be represented by two dashed black lines.

C. Net primary productivity

Previous works used SCC as a proxy variable for NPP [12] because the former is related to the latter and can be obtained by satellite monitoring. However, the NPP depends on other factors as well, and its dependence on SCC is not linear. We use NPP data published by the Oregon State University, computed using the carbon based productivity model [39], [43]. Since NPP data is available, we do not use SCC as a factor in modeling. A map of the NPP data in the CCZ, obtained by averaging over the last two decades, is shown in Fig. 4. There is an underlying assumption in using NPP data, that this variation remained more or less the same at the time when the nodules were formed. This is justified because the NPP variation is governed mainly by variation in sunlight, distance from equator and WCA, which would have been nearly the same during the era when nodules were formed.

D. Distance from WCA, EPR and MMFZ

Based on our observations in subsection II-B, we incorporate the distances from EPR, WCA and MMFZ in the modeling. These are treated as the centers of the identified sources for metal content in nodules to study their relevance to nodule formation. We allow the ANN training to choose the factors of relevance and assign weights accordingly. If a particular factor is effective in explaining nodule parameter variation in the model, it indicates the possible importance of that factor in nodule formation. Conversely, if including a factor does not improve the performance, this indicates that it may not be very relevant. We will see later in our results in section VI that the distance from the MMFZ is not very effective as a factor in modeling.

The locations of the EPR, WCA and MMFZ used in our modeling are indicated in Fig. 5. These were obtained from ISA [12]. The *minimum* distance (in m) of a location in the

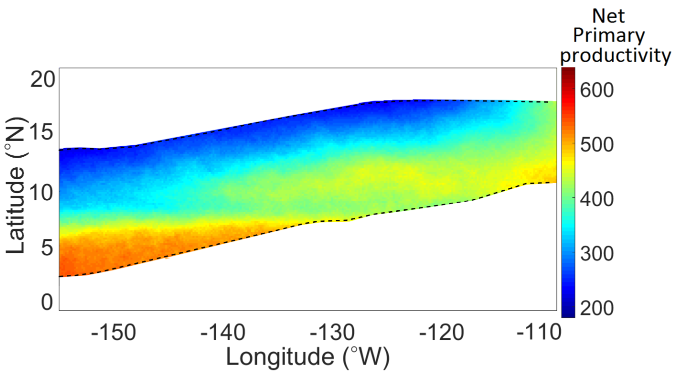

Fig. 4. Net primary productivity variation over the CCZ in mg·C/(m^2·day)

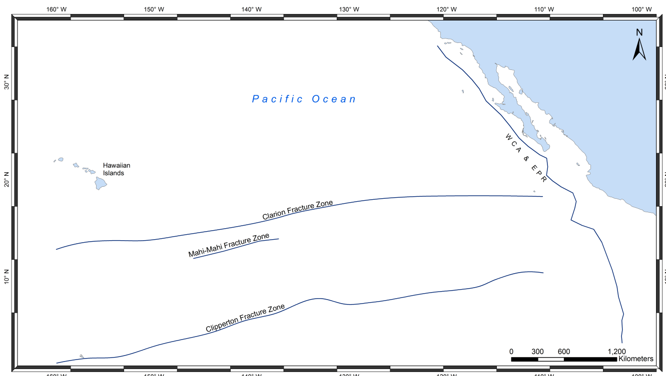

Fig. 5. Locations of EPR, WCA and MMFZ used to compute the factors t_e and t_m.

CCZ from any point along the EPR or WCA is expressed as a factor notated by t_e. Similarly, the *minimum* distance (in m) from the MMFZ is denoted by the factor t_m. This is based on the assumption that the contribution of these sources to nodules at a location, depends on the minimum distance from the sources to this location.

IV. Nodule parameters

We model nodule parameters which are of interest from a commercial and research perspective. These include nodule density and nodule presence which are indicators of the quantity of nodules, and element percentages which are indicators of the quality of nodules.

1) Nodule density or abundance: It is a key factor in determining commercial feasibility for harvesting at a particular site, and defined as the dry weight of FMN in a given 1 m^2 area of the seafloor. Usually, only the top layer (0 to 5 cm) of the sediment is considered for computing abundance as it holds most of the nodule deposits. Also, the top layer is easier for commercial exploitation and hence more relevant when we consider feasibility. Moreover, the nodules on the surface are more easily detected by visual means.
2) Nodule presence probability: This is the probability of finding FMN in a region. Similar variables have been used in the modeling undertaken for the CIEZ [18] and ISA. There is more data on nodule presence available in the open domain than on nodule density. This is because nodule presence can be inferred not just from nodule density values, but also from the descriptions in geophysical data sets provided by sources such as Scripps Institution of Oceanography (SIO) whose data sets contain logs indicating nodule presence or absence.
3) Percentages of elements: Elements which have been identified as being of commercial interest include Ni, Co, Cu and Li [6]. Of these, Ni and Co have been identified as being of particularly high interest. Hence, we consider these elements in this paper. The percentage by weight of these elements in nodules is modeled.

V. Modeling technique

Our data-driven approach towards spatial modeling involves combining information from all known factors in a useful way to make predictions. The modeling should be able to characterize the nonlinear dependence of the nodule parameters on known factors. An ANN can effectively capture this dependence without having to know the nature of variation beforehand, and hence is a good candidate for the modeling. We investigate spatial modeling using a three-layer feed-forward ANN and compare it against other techniques.

A. Collection of data

We collected data for modeling, including bathymetry, sediment-type, NPP, nodule density, element ratios and nodule presence, from online public sources. Table I shows the number of data points we obtained from the open domain for each of the nodule parameters. In Fig. 6, we summarize the locations of the data we collected. Figure 6 (a) shows the locations of the nodule density and nodule presence points and Fig. 6 (b) shows the locations of the Ni % and Co % points. This data has been collated into the respective databases from several cruises, some of which have been published as cruise reports by different institutions [44]–[47]. Studies on chemical analyses and estimation of nodule abundance and morphology via seabed photographs and acoustical means, have also contributed to our understanding of the spatial distributions of these resources [16], [47]–[52]. The sources for each of the factors used by us are shown in table II.

B. Network architecture

An ANN is a powerful computational structure inspired from the brain, that consists of numerous computational units called neurons [22]. Neurons are connected together by weighted links and may have an associated nonlinear transfer function. The network of neurons can function together to perform tasks such as regression, classification and clustering by learning, which is a process of adjusting the weights to achieve the required task. ANNs can approximate any smooth, measurable relationship between input and output vectors by selecting a suitable set of weights. Recent developments in

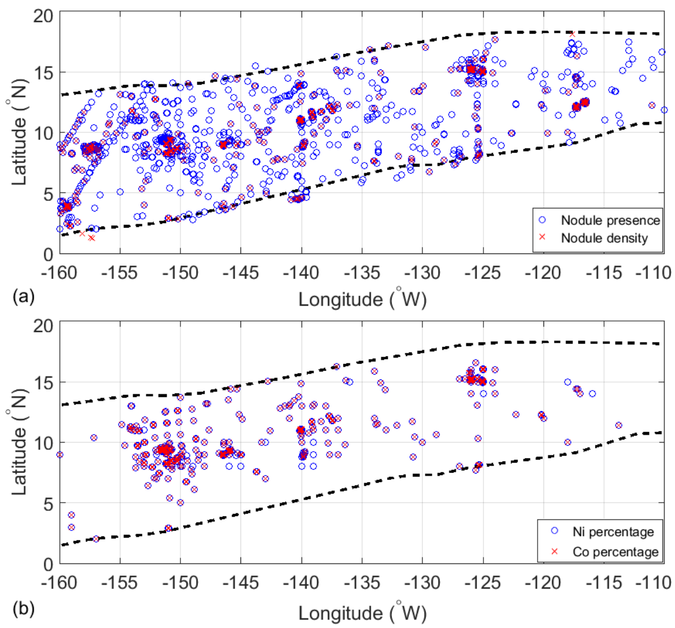

Fig. 6. Locations of data points obtained from the open domain on (a) nodule density and nodule presence, and (b) Ni % and Co %.

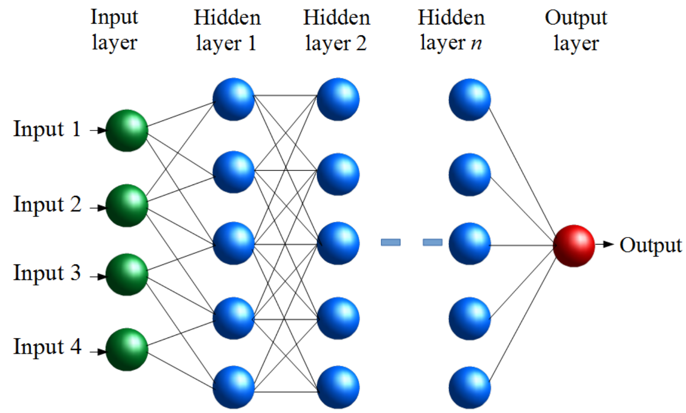

Fig. 7. Example of a 4-input feedforward deep ANN with n hidden layers and one output neuron

ANN have led to success in diverse problems [53]–[55]. We use an ANN to model the nodule parameters as it is known to be effective in pattern recognition.

An ANN consists of layers of neurons, which include an input layer to which information on the 'environment' are supplied, multiple hidden layers, and an output layer which provides the outputs. Each of the input neurons is connected to the neurons in the first hidden layer, which are then connected to the next hidden layer, and so on, until the last hidden layer is connected to the output layer. Training of the ANN involves finding of the best set of weights and biases to each neuron in the hidden layer and output layer, that lead to desired behavior from the ANN [22]. An example of a feed-forward ANN with one input layer, multiple hidden layers and one output layer is shown in Fig. 7.

We use the back-propagation algorithm for training the weights [56]. We employ an optimization method called rmsprop instead of the conventional gradient descent to speed up training. Rmsprop normalizes the current weight gradients by the magnitude of the recent weight gradients to adapt the learning rate [57]. It also incorporates the effect of *momentum* of the learning direction to train towards the optimal solution faster. We aim to minimize the mean-squared-error cost in the case of regression problems (nodule density and element ratios), and softmax cross entropy in the case of nodule presence modeling. Meta-parameters involved in the modeling include the number of hidden layers, neurons, activation nonlinearities, learning rate, momentum decay, epoch size, error cost function, and model selection criteria. Selecting the right meta-parameters involves some heuristic rules and meta-learning [58]. We will now describe our selection of meta-parameters.

Careful selection of the number of hidden layers and neurons is essential for effective modeling. Using too few neurons or layers leads to poor data-fitting, as the ANN is unable to capture the underlying variations in the data adequately. Too many neurons lead to overfitting of the data by making the ANN's prediction specific to the training data alone. Based on our meta-learning, we use two hidden layers and a single neuron in the output layer for the regression-based modeling problems. Taking hints from the results given by Stathakis [59] for a single output neuron, we fix the ratio of neurons in the first hidden layer to the second hidden layer as 5:1. The total number of neurons is heavily data and problem dependent and is chosen through meta-learning. For the regression problems, we use 500 neurons in the first hidden layer.

We treat nodule presence modeling as a classification problem where the ANN has to predict the presence or absence of nodules in the data set. We achieve this by introducing two output neurons in the output layer corresponding to each of these classes, to which the ANN assigns values indicating evidence of nodule presence/absence. These evidences can then be interpreted in terms of nodule presence probability by using a softmax function on the output layer. We obtain the nodule presence probability predictions in this way. We use 25 neurons in the first hidden layer and 5 neurons in the second hidden layer for nodule presence prediction.

We use rectified linear unit (relu) activation nonlinearities in the ANN. These yield good generalization in the performance due to the sparsity introduced into the weight gradients, and make training faster [60]. We use a learning rate that varies exponentially from an initial value $\left(5 \times 10^{-4}\right)$ to a smaller value $\left(1 \times 10^{-6}\right)$ as the training epochs progress. The intuition behind this is that we want the ANN to initially make large, fast changes required to reduce the error from the initial state, and reach the vicinity of the minimum of the training cost function quickly. After that, we slow down the training so that the algorithm can perform fine-tuning via small steps. The neuron weights are initialized randomly from a normal distribution with a variance dependent on the number of neurons in the preceding layer, to prevent saturation of the ANN's capacity during initialization [57].

To obtain an unbiased estimate of the performance of the modeling algorithms, we divide the available data into training,

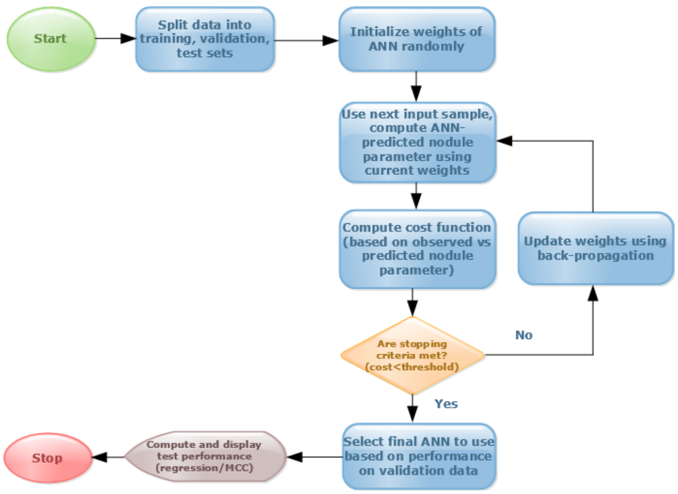

Fig. 8. Flow-chart summarizing the steps and processes involved in ANN-based modeling

validation and test data sets. We select the final ANN model as the one that maximizes the validation performance, which is quantified in terms of regression coefficient for regression problems, and Matthews correlation coefficient (MCC) [61] for classification problems. The model's performance is quantified by using the test data. A flow-chart summarizing the steps in ANN-based modeling is shown in Fig. 8.

C. Methods to improve modeling performance

Our primary challenge is the lack of training data. The relationships between nodule parameters and factors are often nonlinear, complex and partially or fully unknown to us. In the light of these challenges, we adopt several techniques to improve the performance of our modeling. Most of these incorporate prior knowledge of the relationship between the factors and nodule parameters based our understanding of nodule genesis. The techniques we use to improve modeling performance are:

1) Using only magnitude of first-order gradients: We believe that the distinction between upward or downward nature of the slope of the terrain should not matter in nodule formation. This information, indicated by the sign of the first-order gradient, is unnecessary and may lead to overfitting. We limit the training to the magnitudes of the first-order gradients to improve the ANN's performance. However, the sign of the second-order gradients is not ignored as it is required to distinguish between various types of topographic features.
2) Imposing directional symmetry using synthetic data: We assume that the relation between the nodule parameters and topography is independent of the direction considered (eastwards/northwards). In other words, the variation learnt by the ANN with respect to the eastward depth gradients $\Delta_x^1(a,b,\epsilon)$ and $\Delta_x^2(a,b,\epsilon)$, should be the same as that learnt for the northward depth gradients $\Delta_y^1(a,b,\epsilon)$ and $\Delta_y^2(a,b,\epsilon)$ respectively. We encourage the ANN to learn variations independent of the direction by generating an additional set of data from the existing training data by swapping the eastward and northward gradients. This doubles the size of the training data set, and allows the ANN to generalize topographic variations in a direction-independent way.
3) Forcing monotonic variations with t_e and t_m: If we train an ANN to learn variations of nodule parameters based on raw values of t_e and t_m, it may resort to fitting spatial correlations in the training data. This is not very meaningful as the ANN would predict spatially interpolated nodule parameters and end up overfitting. Instead, we require the ANN to learn variations related to genesis of the nodules based on underlying geophysical causes. To force this, we first make the assumption that nodule parameters vary nearly monotonically with respect to t_e and t_m. For example, nodules are more likely to form near the spreading centers than away from them, so nodule density is expected to monotonically decrease with t_e and t_m. ISA [12] use a similar factor in their modeling by employing similar reasoning. Based on our assumption, we force the ANN to learn meaningful models by using inverse exponential features (IEF) derived from t_e and t_m in place of these factors in raw form. When using the IEF, the ANN learns functional dependencies of the form $c_e/t_e^{p_e}$ and $c_m/t_m^{p_m}$, where c_e and c_m are coefficients and p_e and p_m are exponential variables which are learnt by the ANN. In order to prevent the IEF values becoming unbounded when t_e and t_m are close to zero, the minimum values of t_e and t_m are bounded at a value of 100. By modeling using IEFs, the ANN is forced to learn a monotonic relationship with these two factors, and the degree of the variation is learnt from the training data.
4) Using dropout to improve generalization: Dropout is an effective technique to ensure that the ANN generalizes well [62]. It refers to randomly sampling the ANN weights in each training step. This forces each neuron weight to become individually useful, instead of developing complex inter-dependent relationships with other neurons which is likely to lead to overfitting. We use dropout in all ANN models presented in this paper to improve generalization.
5) Dimensionality reduction (DR) of factors: When the factors used in an ANN have correlation amongst themselves, its learning speed is reduced and it does not generalize well [57]. While studying the data, we observed that the four sediment-type factors were highly correlated. We reduce the dimensionality of the sediment-type factors and decorrelate them by using principal component analysis (PCA) prior to the supervised training of the weights. This speeds up the training due to reduction in the number of factors, and also improves the generalization performance. During our modeling, we found a reduced dimensionality of two worked best.
6) Regularization: We further improve the generalization by the ANN by ensuring that the weights learn meaningful smooth variations that are likely to mimic natural phenomena. We do this by imposing a penalty on the

TABLE III
MODELING PERFORMANCE FOR NODULE DENSITY USING COMBINATIONS OF DIFFERENT FACTORS WITH RANDOMLY CHOSEN TEST POINTS. $R_{Del} = 0.561$, $R_{krig} = 0.583$. COLUMNS: A = NPP, B = TOPOGRAPHY, C = SEDIMENT-TYPE (DR TO 2), D = t_e (IEF), E = t_m (IEF), F = SYNTHETIC DATA, G = REGULARIZATION

A	B	C	D	E	F	G	Regression coefficient
✓							0.367
	✓						0.446
		✓					0.505
			✓				0.528
				✓			0.398
✓	✓		✓	✓			0.603
✓	✓	✓	✓	✓			0.606
✓	✓	✓	✓	✓	✓		0.626
✓	✓	✓	✓	✓	✓	✓	0.675

weights in the optimization algorithm, usually in the form of an ℓ_p norm of the weights. We experiment with ℓ_1, $\ell_{1.5}$ and ℓ_2 regularizations in our ANN training.

VI. RESULTS AND DISCUSSION

We investigate the performance of the regression-based modeling in terms of the average test regression coefficient R, which is calculated by averaging over five training runs. We compare the performance of our ANN against predictions made by spatial interpolation techniques. These utilize the spatial correlations between the values of nodule parameters within a region, to predict parameters in unknown locations. Two such techniques that we compare against are:

- Kriging [63] (performance denoted by R_{krig}): Kriging is a conventional technique used in geostatistics to predict a quantity at a specific location using known information of the same quantity at different locations. It is a variant of linear regression [64].
- Linear interpolation via Delaunay triangulation [65] (performance denoted by R_{Del}).

Apart from this, we also benchmark our outputs against the predictions given by ISA [12]. Note that the predictions by ISA were done using a larger amount of data, including that obtained from proprietary sources. The ISA predictions use 61583, 8360 and 8249 points for nodule density, Ni% and Co% respectively, whereas only a fraction of these data points are available to us in the open domain for these nodule parameters.

A. Nodule density

First, we consider modeling of the nodule density variation across the CCZ. We randomly divide the available data points into training, validation and test sets in the ratio 70:15:15. Since the test points are randomly chosen from all data available for the CCZ, the test performance is indicative of the capability of the ANN to model large-scale variation of nodule density over the CCZ.

We investigate the performance using each of the factors mentioned in section III, and some combinations of these factors. We summarize these performances in table III. In this table, each row represents a training scenario performed with a certain set of factors or modeling techniques (such as synthetic data or regularization). The factors/techniques used are indicated by tick-marks in their respective columns. The corresponding test performance is indicated on the right-most column. This interpretation applies to all such tables shown henceforth. In the tabulated results presented henceforth, we do not list the performances using all combinations of the factors, as the list is quite large and does not provide any significantly new insights. The tabulated performance is based on an ANN that uses IEF of t_m and t_e, uses the magnitude of the first-order gradients, and uses sediment-type factors after reducing their dimensionality by two via PCA.

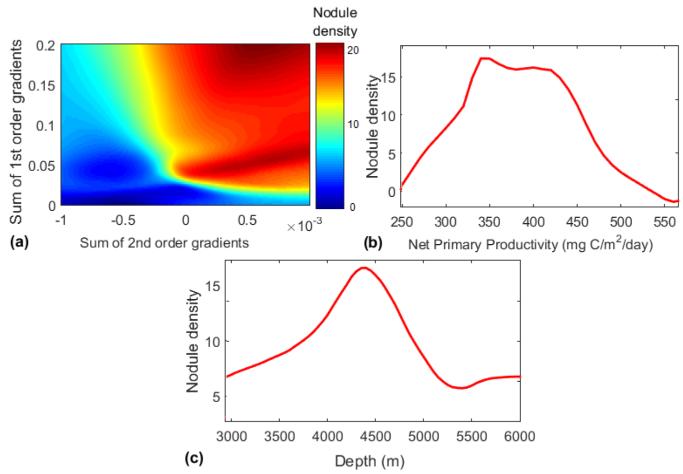

Fig. 9. Modeled variation of nodule density with topographic factors. The variation is plotted against (a) $\Delta^1 = \Delta^1_x + \Delta^1_y$ and $\Delta^2 = \Delta^2_x + \Delta^2_y$, (b) NPP and (c) depth. Average parameter values are $\Delta^1_x = \Delta^1_y = 0.04$, $\Delta^2_x = \Delta^2_y = 6 \times 10^{-5}$, $NPP = 368.3$ mg·C/(m^2·day), $d = 4630$ m,$S_t = 0.1$,$S_p = 0.33$,$S_c = 0.21$,$S_s = 0.36$, $t_e = 3.03 \times 10^6$ m,$t_m = 8.849 \times 10^6$ m unless otherwise specified.

For the nodule density data set considered, Delaunay triangulation yields a test performance $R_{Del} = 0.561$, whereas kriging yields $R_{krig} = 0.583$. In table III, test regression coefficients obtained using the individual factors indicate how effective these are in modeling *when used in isolation* and not combined with information from other factors. Often, using a single factor may not provide enough information on nodule formation, and using certain combinations of these factors may yield better performance of the ANN model. In the current case, combining eight input factors consisting of t_e, t_m, topography, and NPP, yields $R = 0.603$. Adding the sediment-type factors along with these improves the performance by only 0.5%. We also observe the following:

1) PCA-based DR of sediment-type factors improves the performance by 19% over the case when raw sediment-type factor inputs are used.
2) Replacing the signed values of the first-order gradients with their magnitudes improves the performance by 28%.
3) Use of IEF instead of the raw values of t_m and t_e as factors, improves the performance by 31%.
4) Adding synthetic data points to incorporate directional symmetry yields a performance of $R = 0.6264$, which is 3.4% better than the case when no synthetic data points

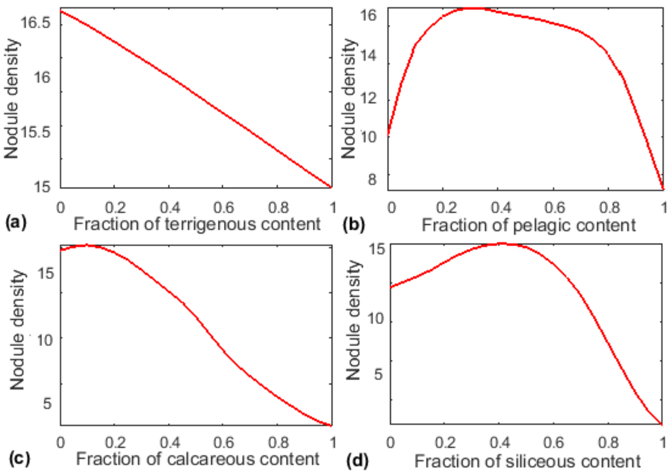

Fig. 10. Modeled variation of nodule density with fraction of (a) terrigenous, (b) pelagic, (c) calcareous and (d) siliceous content in sediment. Average parameter values are $\Delta_x^1 = \Delta_y^1 = 0.04$, $\Delta_x^2 = \Delta_y^2 = 6 \times 10^{-5}$, $NPP = 368.3$ mg·C/(m^2·day), $d = 4630$ m, $t_e = 3.03 \times 10^6$ m, $t_m = 8.849 \times 10^6$ m unless otherwise specified.

are used.

5) Regularizing the weights with an $\ell_{1.5}$ norm improves the performance by 7.7%.

We note that for the current data set, ANN modeling using any one factor alone does not perform as well as the interpolation techniques. However, when all the related factors we discussed are used for prediction, the ANN is able to yield better performance than the interpolation approaches which utilize spatial correlations. Overall, the regularized ANN trained with synthetic data outperforms Delaunay triangulation by 20.3% and kriging by 15.8%, and yields a performance $R = 0.675$.

In Fig. 9, we briefly study the variations of nodule density learnt by the ANN with respect to the topographic and NPP input factors. Figure 9 (a), which plots the variation of nodule density against $\Delta^1 = \Delta_x^1 + \Delta_y^1$ and $\Delta^2 = \Delta_x^2 + \Delta_y^2$, gives us an idea about the model learnt by the ANN with respect to the depth gradients. The plots in Fig. 9 essentially represent 2-D slices or 1-D line cuts through the 10-D factor space in which the ANN has learnt its variation for the trained model. The model output is averaged over ANNs obtained from three training runs with high validation performance. Apart from the factors against which the variation is plotted, we set the values of all other factors at their averages over the entire collected data set unless otherwise mentioned.

Figure 9 indicates that the ANN models the nodule density variation with the NPP and depth as being non-monotonic. It predicts that the highest nodule density occurs at NPP of 330 to 420 mg·C/(m^2·day) and a depth of around 4300 m. This agrees with the observation made by Kotlinski [40]. Nodule density decreases for depths shallower than 4300 m due to the dilution caused by carbonate precipitation occurring above the CCD [19]. The non-monotonic variation with NPP is due to the interplay between two opposing trends: improved nodule formation due to biogenic sedimentation, and increasing dilution of metals from excess biogenic sedimentation. At very low levels of biological activity, the supply of metals to the seafloor is insufficient to produce nodule deposits [20]. However, in regions with relatively high biological activity, the flux of organic matter will exceed the rates at which the benthic nodule-forming processes can extract metals.

The variation with first-order gradient is somewhat increasing in nature. This indicates that highest nodule density is found at locations with large first-order gradient and positive second-order gradient. The interpretation is that areas beside abyssal hills are expected to have higher nodule density, which matches the observations made by previous researchers and validates our ANN model.

The ANN model also indicates that the IEF derived from t_e contributes significantly in modeling the variation across the CCZ. The average values of the coefficients learnt by the ANN are $c_e = 4.8 \times 10^5$ and $p_e = 0.69$. The IEF from t_m contributes to a lower degree with $c_m = 151$ and $p_m = 0.52$.

In Fig. 10 we plot the modeled variation of nodule density against the sediment fractions. This is obtained by averaging over three training instances with high validation performance. The values for other parameters are the same as those for Fig. 9. Figure 10 indicates that nodule density decreases with an increase in the calcareous or large terrigenous content in the sediment. This observation agrees with ones made by several authors earlier. The ANN models the variation with pelagic clay and siliceous sediment as non-monotonic, with the maximum nodule density occurring at intermediate values of S_p and S_s. Though this contrasts with the observation of some authors that nodule density is highest in areas with pelagic clay or siliceous sediment, studies by China Ocean Mineral Resources R&D Association record that the highest nodule density is supported by siliceous-calcareous ooze, rather than pure siliceous ooze [12]. Our model seems to support this statement, and predicts that the highest nodule density is found in siliceous-calcareous sediment with $S_c = 0.2$, $S_p = 0.3$ and $S_s = 0.5$.

In Fig. 11, we plot the nodule density variation predicted over the CCZ by the ANN. The prediction is done only in areas where the water depth is below the CCD, which we identify using the map given by ISA [12]. This is because nodule formation is impeded in areas located higher than the CCD. The white regions within the CCZ zone in Fig. 11 indicate these regions. We will follow this convention in all subsequent prediction maps in this section.

Note that the model predicts a large band of high nodule density in the center of the CCZ, and lower nodule density as one goes westwards from the EPR or southwards from the MMFZ. There is a region of high nodule density at a belt around 13° N, between 121° W to 127° W. We see a belt of high concentration as we move southwestwards from 13° N, 127° W. Specifically, there are regions of high concentration spread around 13° N, 127° W and 12.5° N, 135° W. These features are consistent with the observations made so far in the CCZ as recorded by ISA [12], showing that our predictions correlate well with real-world data. Note that our training data set contained very few data points in some of the locations where features similar to ISA's predictions were observed, such as the region north of 14.5° N and between 110° W to 124.8° W, and the low nodule-density region to the southwest

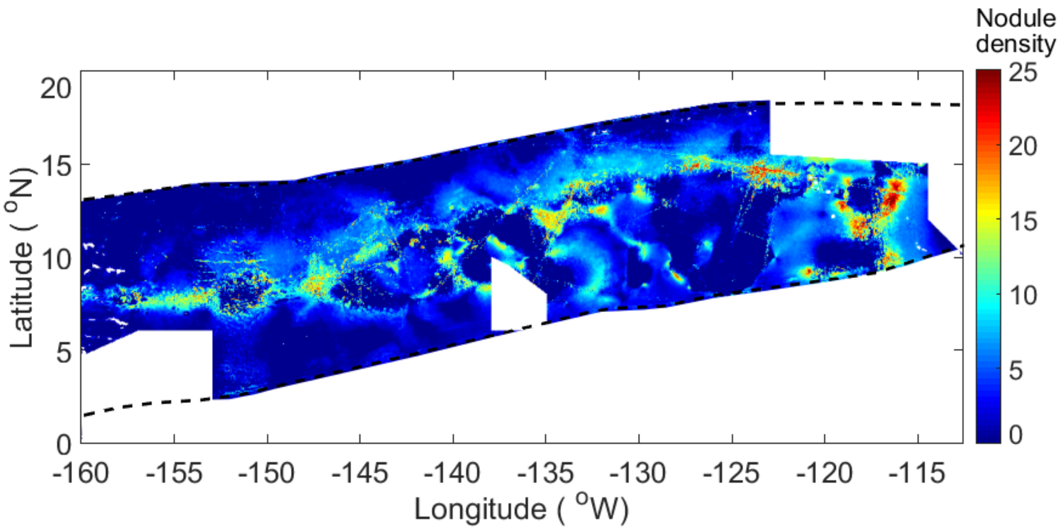

Fig. 11. Nodule density variation across CCZ predicted using ANN model (in kg/m^2).

TABLE IV
MODELING PERFORMANCE FOR NODULE DENSITY USING COMBINATIONS OF DIFFERENT FACTORS WITH TEST POINTS WITHIN A SMALL REGION. $R_{Del} = -0.302, R_{krig} = -0.365$. COLUMNS: A = NPP, B = TOPOGRAPHY, C = SEDIMENT-TYPE (DR TO 2), D = t_e (IEF), E = t_m (IEF), F = SYNTHETIC DATA, G = REGULARIZATION

A	B	C	D	E	F	G	Regression coefficient
	✓						0.275
		✓					0.035
			✓				0.137
				✓			0
	✓		✓				0.291
	✓			✓			0.271
	✓		✓		✓		0.338
	✓		✓		✓	✓	0.457

TABLE V
MODELING PERFORMANCE FOR NI % USING COMBINATIONS OF DIFFERENT FACTORS. $R_{Del} = 0.082, R_{krig} = 0.135$. COLUMNS: A = NPP, B = TOPOGRAPHY, C = SEDIMENT-TYPE (DR TO 2), D = t_e (IEF), E = t_m (IEF), F = SYNTHETIC DATA, G = REGULARIZATION

A	B	C	D	E	F	G	Regression coefficient
✓							0.238
	✓						0.277
		✓					0.068
			✓				-0.35
				✓			0
✓	✓	✓	✓				0.29
✓	✓	✓	✓	✓			0.278
✓	✓	✓	✓		✓		0.313
✓	✓	✓	✓		✓	✓	0.377

corner of CCZ, east of 153° W. The only data available in some of these regions was on nodule presence or absence. This indicates that the ANN predicted these nodule density features via effective learning using the input factors, and did not just interpolate them. One region where our prediction trends do not match data collected by ISA is the region around 7° N, 132° W. Our predictions also indicate a region of low nodule density in the western edge of CCZ due to its large distance from the spreading centers. This contrasts with the observed data that indicates a region of moderate nodule density here. This suggests a limitation in our modeling due to the functional form of the IEF used by us. In the future, we may be able to reduce this deviation by using separate factors for river run-off from the WCA and distance from the EPR, as they contribute to different types of metals and affect nodule genesis differently. We may also be able to improve the performance by using more theoretically justified models for spreading of metals from their sources.

So far we have elucidated the ability of our trained ANNs to predict nodule density variations on a large scale across CCZ. Sometimes, during exploration, it is required to make small-scale predictions within a small region. We explore the performance of modeling nodule density points within a square region that is 0.8° wide in latitude and 1° in longitude. We train the ANN with 378 data points, validate using 34 points, and test using 42 points. We have high resolution bathymetry data in this region, which we use to model the nodule density variations at smaller scales.

We summarize the performance in table IV. Note that topographic factors are more effective than NPP, sediment-type or distance from EPR or MMFZ in explaining spatial variations at small regional scales. When used alone, only topographic factors seem to be effective in explaining the variations. This is because at small distance scales, only topographic and sediment-type fluctuations may influence nodule density variation. The modeling performance improves when we club the topographic factors together with the IEF derived from t_e. None of the other factors contribute to improvement in this performance

Sediment-type information does not contribute to modeling performance in this case. This may be because, since sediment-type data in this region was not available to us, we obtained it by kriging from data available from other regions of CCZ. This kriged data does not contain much information on small-scale variations and is not accurate enough to provide information for modeling, though it may be useful for a coarse prediction at larger scales. Better sediment-type data may enable us to improve the modeling performance further.

We also find that:

1) PCA-based DR on the sediment-type factors improves the performance by 13.2% over the case when raw inputs are used.
2) Use of IEF instead of using the raw values of t_e improves the performance by 2%.
3) Adding synthetic data to incorporate directional symmetry improves the performance by 16.2%.
4) ℓ_2 norm-based weights regularization improves the performance by 35%.

Overall, the regularized ANN trained with synthetic data yields $R = 0.46$. This performance is significantly higher than that obtained from Delaunay triangulation and kriging, which predict trends contrary to the test data. Our results so far and investigations with other data sets show that using magnitudes of first-order gradients, dropout, DR of sediment data using PCA, and using IEF instead of directly using t_m and t_e, work effectively. Henceforth, in all our results we describe results using sediment-type factors with DR, magnitudes of first-order gradients, dropout and IEF in the modeling. We will not discuss the improvement due to these techniques any further in this section.

B. Nickel percentage

We now discuss the modeling of Ni % in the nodules conditional on the presence of the nodules. We train the ANN using 411 data points, validate using 90 points, and test using 71 points. The performances of ANN modeling using different factors, and that of spatial interpolation methods, are summarized in table V. We find that all the factors considered by us except t_m contribute to improving the ANN's performance in modeling the Ni %. Topographic factors are individually the most effective in explaining the variation in this case.

We also find that:

1) Adding synthetic data to incorporate directional symmetry improves the performance by 7.9%.
2) ℓ_2 norm-based weights regularization improves the performance by 20.5%.

Overall, the ANN with synthetic data and regularization yielded $R = 0.377$. This performance is significantly better than that of Delaunay triangulation and kriging for the Ni % data set.

In Fig. 12, we briefly study the variations of Ni % learnt by the ANN with respect to the input factors used in the modeling. We set the values of the factors not plotted against, at their averages over all the collected data points. Figure 12 shows that the ANN models the Ni % variation to be non-monotonic with NPP, and predicts the highest Ni % to occur around NPP $= 410$ mg·C/(m^2·day). This dependence is similar to the non-monotonic one observed by other models [12]. This variation can be explained by the balance between increasing supply of metals due to increase in NPP, and dilution of metals due to excess biogenous sedimentation, as we described for the case of nodule density. The Ni % increases with depth, suggesting that more Ni is found in deeper valleys. The variation with topography shows that Ni % is higher in regions with low first-order gradients and negative second-order gradients, which indicate plains and gently-sloping valleys. This model is consistent with the geological explanation for the entry of Ni into nodules via diagenetic processes, which dominates in regions such as valleys where sedimentation rates are low.

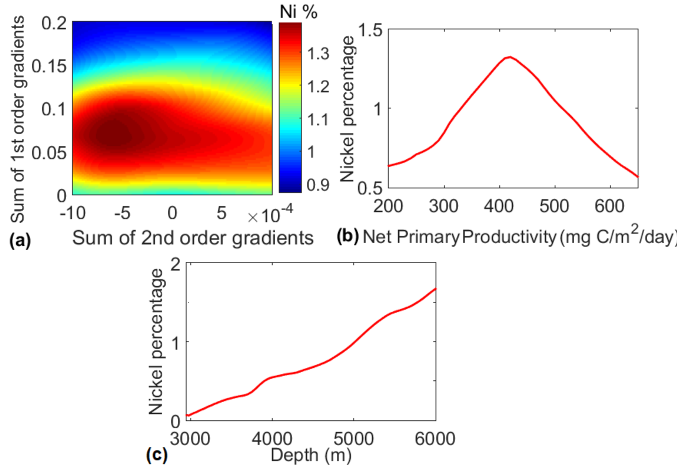

Fig. 12. Modeled variation of Ni % with topographic factors. The variation is plotted against (a) $\Delta^1 = \Delta^1_x + \Delta^1_y$ and $\Delta^2 = \Delta^2_x + \Delta^2_y$, (b) NPP and (c) depth. Average parameter values are $S_t = 0.14$, $S_p = 0.35$, $S_c = 0.2$, $S_s = 0.31$, $t_e = 3.91 \times 10^6$, $t_m = 1.98 \times 10^6$, $d = 5048$ m,$\Delta^1_x = \Delta^1_y = 0.022$, $\Delta^2_x = \Delta^2_y = 8.1 \times 10^{-5}$/m and $NPP = 338$ mg·C/(m^2·day).

The ANN model also indicates that the IEF derived from t_e contributes significantly to the variation across CCZ, yielding an average value for the coefficients as $c_e = -3.4 \times 10^5$ and $p_e = 0.73$. The IEF from t_m contributes to the variation to a smaller degree with $c_m = -478$ and $p_m = 0.89$.

We generate a prediction map of the conditional Ni % in nodules over the CCZ area, using the ANN model trained with all the factors. This map is plotted in Fig. 13. The trends of the variation predicted by us is somewhat similar to those observed across the entire CCZ as described in the ISA report [12], even in areas where we had very scarce training data. This includes the western zone of CCZ ($> 153°$ W) and the southern quarter of CCZ.

C. Cobalt percentage

We now discuss the performance of modeling the Co % in the nodules conditional on the presence of the nodules. We train the ANN using 357 data points, validate using 81 points, and test using 71 points. We summarize the performance of modeling using different factors and spatial interpolation methods in table VI.

We note that only NPP and topography are useful in making predictions of Co % *when used individually*, but when combined together with t_e (IEF), the ANN yields a better performance of $R = 0.306$. Observe that the dependence of Ni % on NPP is higher than that of Co %, and the opposite

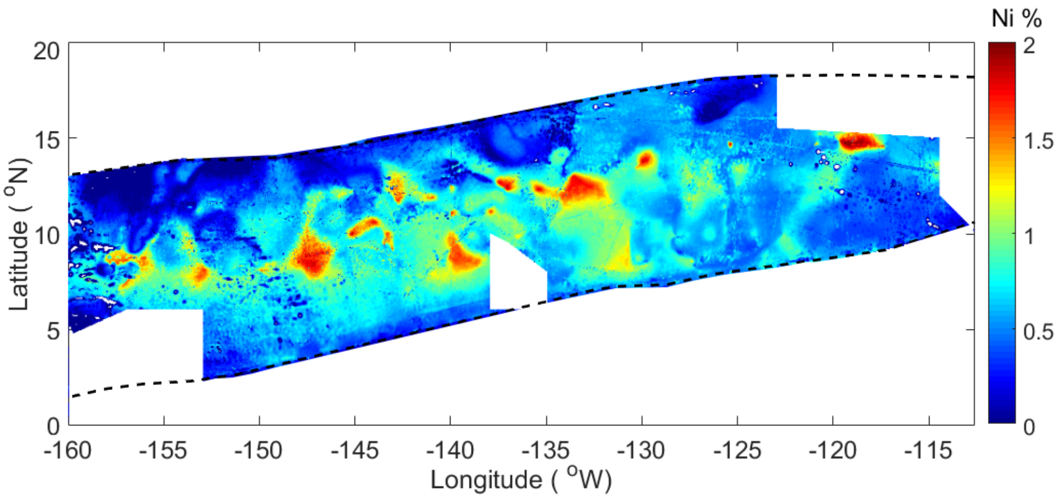

Fig. 13. Conditional Ni % across CCZ predicted using ANN model.

trend is noted for topography. This is because NPP is directly related to the Ni % as it determines the supply rate of Ni to the nodules. On the other hand, NPP may be only indirectly related to the entry of Co into the nodules by influencing the nodule formation mechanism. This observation is in line with that noted by Frazer and Fisk [15]. We also find that:

1) ℓ_2 norm-based weights regularization improves the performance by 21% .
2) Modeling using synthetic data to incorporate directional symmetry does not yield a performance improvement. On the contrary, it leads to a degradation. The reason for this is not obvious to us. It could be due to asymmetricities arising from directional effects that we have not incorporated. One such possible cause is that of benthic currents, which lead to contrasting effects on nodule parameters on different sides of a seamount in their path [41]. These may affect the symmetry of processes such as the spreading of Co ions from volcanogenic sources or the formation of hydrogenetic nodules.

Overall, the regularized ANN yielded a performance of $R = 0.371$. This is 61.9% better than Delaunay triangulation and 23.5% better than kriging.

In Fig. 14, we briefly study the variations of Co % with respect to the input factors learnt by the ANN model. We set the values of the factors not plotted against, at their averages over all the collected data points. Figure 14 indicates that the ANN models the Co % variation to be monotonically decreasing with NPP and depth, and increasing with the first-order gradient. The variation with topographic factors indicates that Co is abundantly found on or beside abyssal hills, rather than on plains. This is in line with our physical understanding of the entry of Co, which is higher near volcanic and hilly areas. In such areas, large topographic variations and the presence of large number of nuclei in the form of rocks, lead to dominance of hydrogenesis. This, in turn, increases the supply of Co to nodules formed in these regions. The inverse dependence of Co on NPP could be an indirect effect due to the influence of NPP on the mechanism of nodule genesis.

TABLE VI
MODELING PERFORMANCE FOR CO % USING COMBINATIONS OF DIFFERENT FACTORS. $R_{Del} = 0.185$, $R_{krig} = 0.3$. COLUMNS: A = NPP, B = TOPOGRAPHY, C = SEDIMENT-TYPE (DR TO 2), D = t_e (IEF), E = t_m (IEF), F = SYNTHETIC DATA,G = REGULARIZATION

A	B	C	D	E	F	G	Regression coefficient
✓							0.197
	✓						0.249
		✓					0.01
			✓				0.05
				✓			0.06
✓	✓		✓				0.306
✓	✓		✓		✓	✓	0.337
✓	✓		✓			✓	0.371

In Fig. 15, we plot the conditional Co % in nodules over the CCZ area predicted by the trained ANN model. The variation has similarities to that described by ISA, even in areas where we did not have training data. Some of the similarities include the belt of high Co in the northwest (around $155°$ W) and the northeast (around $125°$ W) with an area of low Co % in between. Both the models predict that the areas to the east and southwest have low Co %. However, our model predicts a region of moderate Co in the southeast area which is a feature not seen in the ISA report. This is because of the low NPP in this region, and its proximity to the EPR. Note that the ANN has learnt that the Co % inversely varies with NPP, which may not be entirely accurate in forming the prediction. In the future, we can address this deviation by modifying the ANN model's dependence on NPP and sediment-type factors to make them more useful and accurate. Introducing the CCD as a factor may also help improve the modeling, because the southward variation of Co % is probably more dependent on the CCD rather than on NPP as the ANN has learnt currently.

D. Nodule presence

We now model the probability of nodule occurrence using ANN. We treat this as a classification problem, in which the ANN attempts to predict presence or absence of nodules

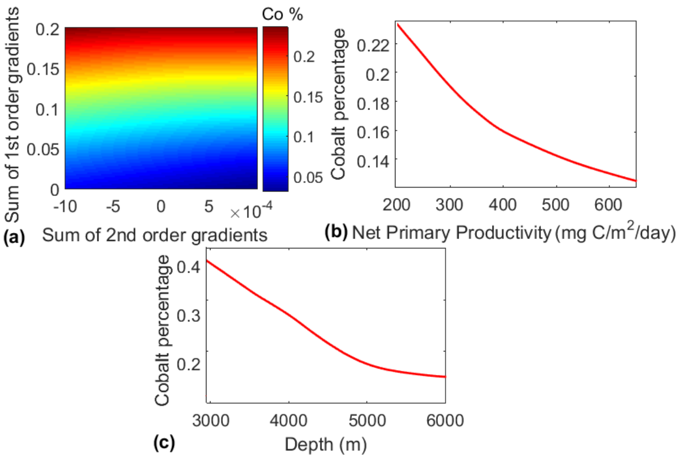

Fig. 14. Modeled variation of Co % with topographic factors. The variation is plotted against (a) $\Delta^1 = \Delta^1_x + \Delta^1_y$ and $\Delta^2 = \Delta^2_x + \Delta^2_y$, (b) NPP and (c) depth. Average parameter values are $S_t = 0.13$,$S_p = 0.35$,$S_c = 0.19$,$S_s = 0.31$, $t_e = 3.91 \times 10^6$, $t_m = 1.98 \times 10^6$, $d = 5048$ m, $\Delta^1_x = \Delta^1_y = 0.022$, $\Delta^2_x = \Delta^2_y = 8.1 \times 10^{-5}$/m and $NPP = 338$ mg·C/(m^2·day).

TABLE VII
MODELING PERFORMANCE FOR NODULE PRESENCE USING COMBINATIONS OF DIFFERENT FACTORS. COLUMNS: A = NPP, B = TOPOGRAPHY, C = SEDIMENT-TYPE (DR TO 2), D = t_e (IEF), E = t_m (IEF), F = SYNTHETIC DATA, G = REGULARIZATION

A	B	C	D	E	F	G	MCC
✓							0.251
	✓						0.100
		✓					0.005
			✓				0.051
				✓			0.02
✓	✓	✓	✓	✓			0.262
✓	✓	✓	✓	✓	✓		0.271
✓	✓	✓	✓	✓	✓	✓	0.279

at a particular site. The data we collected contains many more points indicating nodule presence, than those indicating absence. Hence, we use MCC as a performance metric because it is considered a balanced measure of classification performance. The MCC is a suitable metric when the two classes being considered are of unequal sizes [61]. It is also a good indicator of the quality of the confusion matrix of the classifier in such a case, and thus a good choice as a performance metric. Apart from the MCC, we also evaluate the methods in terms of the area under the curve (AUC) of their receiver operating characteristics (ROC) [61].

We divide the available data in the ratio 70:15:15 for training, validation and testing. Y denotes the MCC of ANN with test data points. We compare the performance of the ANN against two other standard classification methods found in the literature, namely logistic regression (LR) and the frequency ratio method (FRM) [66], [67]. For fairness of comparison, the FRM and LR methods use both the training and validation sets for modeling. We summarize the ANN's performance in modeling nodule presence with different factors in table VII.

We see that when used alone, the NPP is the most effective factor in explaining the variation of nodule presence for the given test data set. All the other factors are effective to

TABLE VIII
MODELING PERFORMANCE FOR NODULE PRESENCE COMPARED FOR DIFFERENT MODELING TECHNIQUES

Method	Matthews correlation coefficient	Area under ROC curve
ANN	0.279	0.72
FRM	0.18	0.725
LR	0.054	0.51

a smaller degree, and t_m seems to be the least effective. The best performance achievable with all the factors and no regularization or synthetic data, is $Y = 0.262$. We also note that:

1) Adding synthetic data to incorporate directional symmetry improves the performance by 3.29%.
2) $\ell_{1.5}$ norm-based weights regularization improves the performance by 3.1%.

Overall, the regularized ANN trained with synthetic data yields a performance of $Y = 0.279$.

In table VIII we tabulate the performances of ANN, FRM and LR in terms of their MCC and AUC in nodule presence modeling. We see that the ANN's MCC is significantly higher than the LR method, and 55% better than the FRM. In terms of AUC, the ANN is comparable to the FRM and better than the LR method.

In Fig. 16, we plot the nodule occurrence probability across the CCZ predicted by the trained model. The probability is inferred from the evidence values obtained for nodule presence/absence by the ANN, by introducing a softmax probability layer at the output of the classification ANN [60]. This layer converts the evidence values to a value between 0 and 1 which can be interpreted as the predicted probability of nodule occurrence.

The plot in Fig. 16 compares well against the prediction of nodule occurrence probability given in the ISA report. This validates the effectiveness of ANN in generalizing the predictions with the small number of available data points.

VII. CONCLUSION

We elucidated a methodology for data-driven spatial modeling of nodule parameters in the CCZ by employing artificial neural networks. We successfully modeled the nodule density, percentage by weight of nickel and cobalt, and nodule presence probability, using a three-layer feedforward network. We demonstrated this in terms of performance measures based on test data sets chosen within CCZ. The ANN is able to efficiently combine diverse surrogate parameters related to nodule genesis and characterize their nonlinear dependence on the nodule parameters to generate predictions. We demonstrated using groundtruth data collected from open-domain databases, that the ANN-based model outperforms kriging and interpolation methods. We have not conducted additional surveys to collect groundtruth nodule data from the field to validate our results.

ANN-based modeling can be employed by industry engineers and/or enterprises as a powerful tool for analyzing spatial distributions of deep-sea minerals in the future. We

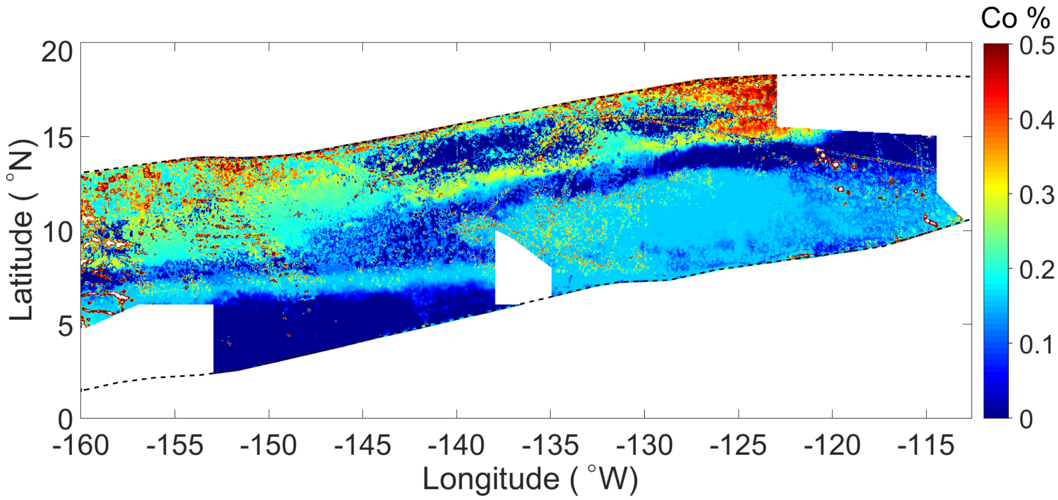

Fig. 15. Conditional Co % across CCZ predicted using ANN model.

demonstrated the usability of this technique through comparison against previously published results. We validated our results by comparing our predictions against those by ISA, and by comparing the functional variations and trends learnt by the model against those observed in the literature. This serves as a first trial in the application of this method to the field of deep-sea mining.

Strategies that helped improve modeling performance include addition of synthetic data to force directional independence of nodule parameter variation, using the magnitudes of the first-order gradients, forcing a monotonic dependence of the nodule parameters with the distance from EPR, WCA and MMFZ, reducing the dimensionality of sediment data, regularization and dropout.

Most of the factors used in the modeling were demonstrated to be effective in prediction. Topographic factors work consistently well and were vital in making small-scale predictions. NPP was also an important factor for prediction in most cases. The factor t_e led to performance degradation when used as a raw factor in modeling, but yielded small improvements when a monotonic dependence was enforced in the model. The factor t_m yielded marginal or no performance in modeling of most of the nodule parameters. This could indicate the MMFZ might not have played a vital role in nodule formation.

The key points in our work that set it apart from previous works on nodule parameter modeling are the following:

1) A full description of the ANN model and its setup, including network architecture, factor selection and processing, learning algorithm, regularization techniques and meta-parameters used in training. We detailed our modeling in a way that allows a reader to reproduce these results, which no published literature provides as far as our review covers.
2) We demonstrated how limited data can be efficiently used for modeling. As a comparison, even though we used only a fraction of the data points used by ISA in their report, our results are comparable. The smart processing techniques we used enabled us to achieve this.
3) We enhanced the use of topographic and geophysical factors as numerical quantities based on obtained data, in contrast to the categorical approach used in previous modeling attempts. These approaches to factor selection also contributed to efficient use of the limited data.
4) Our approach to incorporate the distance from the EPR and WCA as factors varies from previous attempts at modeling nodule parameters. Our factor is modeled in an IEF form, with the exponential decay factor *learnt from the data* rather than chosen manually.
5) We studied the use of an additional factor, the distance from the MMFZ, which has not been dealt with in the nodule parameter modeling literature.
6) We used NPP as an input factor rather than SCC, because the former reflects more directly the biological activity at the sea surface that contributed to nodule formation.

Our performance indicators demonstrate the fair accuracy of our ANN model despite limited data available for training. Based on this, we believe that our model is a suitable tool to make an initial assessment for resources prior to exploration. We expect that the predictive power of the model can be further improved if additional data from explorations can be incorporated. Collecting additional nodule data to validate the model would be a natural extension to this work. Further improvements could be possible by harnessing the power of modern deep learning techniques to boost performance.

VIII. Acknowledgment

The authors thank the National Research Foundation, Keppel Corporation and National University of Singapore for supporting this work done in the Keppel-NUS Corporate Laboratory. The conclusions put forward reflect the views of the authors alone, and not necessarily those of the institutions within the Corporate Laboratory.

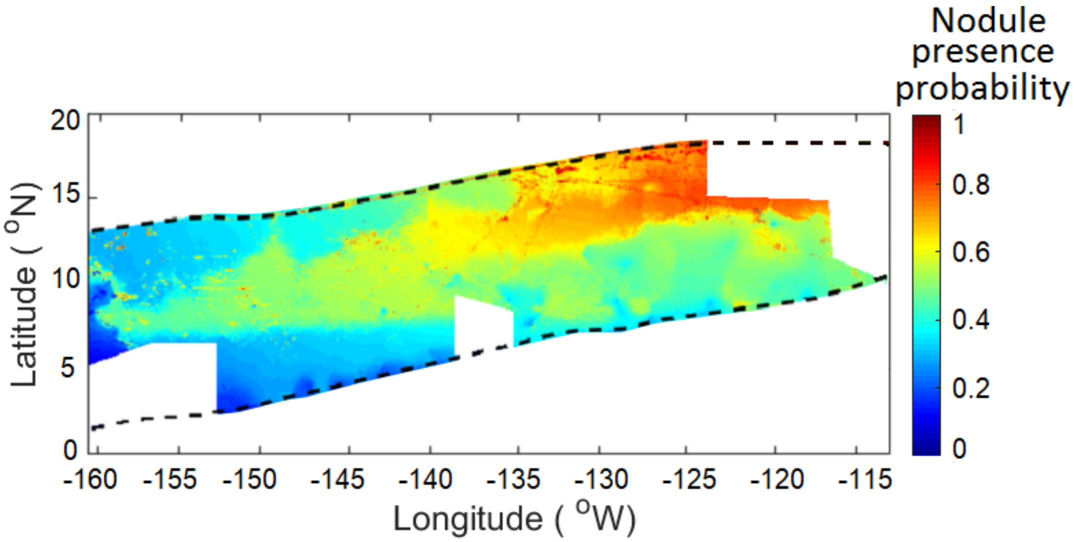

Fig. 16. Nodule presence probability across CCZ predicted using ANN model.

Hari Vishnu (S'04-M'08) has been at the Acoustic Research Laboratory, National University of Singapore since 2013. He received the B.Tech. degree in electronics and electrical engineering from the National Institute of Technology, Calicut, India, in 2008 and the Ph.D. degree in computer engineering from the Nanyang Technological University, Singapore, in 2013. His Ph.D. research involved development of improved underwater signal processing algorithms. These included acoustic modeling, detection and localization, vector sensor processing, and robust signal processing in non-Gaussian noise.

He is currently a research lead, and his research interests include machine learning for marine applications, active sonar, bio-acoustics, acoustic propagation modeling, and robust signal processing.

Dr. Vishnu was a reviewer for several reputed international journals. He is currently the Secretary of the IEEE Singapore AUV Challenge Committee and the IEEE Oceanic Engineering Society, Singapore chapter.

Bharath Kalyan (M'05) is currently with Acoustic Research Laboratory (ARL), TMSI, National University of Singapore where he manages myriad projects on Deepsea mining and marine robotics. Prior to joining ARL, he was a research staff at Intelligent Robotics Lab, Department of Electrical and Electronic Engineering (EEE) at Nanyang Technological University (NTU), Singapore where he worked on various underwater projects, primarily focusing on underwater sensing and navigation for surface and undersea vehicles. He was awarded a PhD by NTU for his research work on autonomous underwater vehicle navigation. His research interests include machine learning, deepsea mining, co-operative marine robotics, AUV navigation, target tracking, random finite sets.

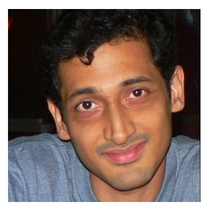

Mandar Chitre (S'04-M'05-SM'11) received B.Eng. and M.Eng. degrees in electrical engineering from the National University of Singapore (NUS), Singapore, in 1997 and 2000, respectively, the M.Sc. degree in bioinformatics from the Nanyang Technological University (NTU), Singapore, in 2004, and the Ph.D. degree in underwater communications from NUS, in 2006. From 1997 to 1998, he worked with the ARL, NUS in Singapore. From 1998 to 2002, he headed the technology division of a regional telecommunications solutions company. In 2003, he rejoined ARL, initially as the Deputy Head (Research) and is now the Head of the laboratory. Dr. Chitre also holds a joint appointment with the Department of Electrical and Computer Engineering at NUS as an Assistant Professor. His current research interests are underwater communications, autonomous underwater vehicles, model based signal processing and modeling of complex dynamic systems.

Dr. Chitre has served on the technical program committees of the IEEE OCEANS, WUWNet, DTA and OTC conferences and has served as reviewer for numerous international journals. He was the chairman of the student poster committee for IEEE OCEANS 06 in Singapore, and the chairman for the IEEE Singapore AUV Challenge 2013. He is currently the IEEE Ocean Engineering Society technology committee co-chair of underwater communication, navigation and positioning.

Varadarajan Ganesan received his B.Eng. and M.Eng. degrees in Mechanical and Electrical and Computer Engineering respectively from the National University of Singapore (NUS). His Masters thesis involved developing a robust underwater obstacle detection and avoidance system. He was working at the Acoustic Research Laboratory (ARL), NUS, as a Research Engineer. He has now moved to the industry and is working as a data scientist.

References

[1] T. Marjoram, H. Cameron, G. Ford, A. Garner, and M. Gibbons, "Manganese nodules and marine technology," *Resources Policy*, vol. 7, no. 1, pp. 45–57, mar 1981.

[2] H. Kunzendorf, W. Pluger, and G. Friedrich, "Uranium in pacific deep-sea sediments and manganese nodules," *Journal of Geochemical Exploration*, vol. 19, no. 1-3, pp. 147–162, dec 1983.

[3] G. N. Baturin, *The Geochemistry of Manganese and Manganese Nodules in the Ocean*. Dordrecht: Springer Netherlands, 1988, vol. 2.

[4] G. Glasby, "Deep Seabed Mining: Past Failures and Future Prospects," *Marine Georesources & Geotechnology*, vol. 20, no. 2, pp. 161–176, apr 2002.

[5] J. Hein, K. Mizell, A. Koschinsky, and T. Conrad, "Deep-ocean mineral deposits as a source of critical metals for high- and green-technology applications: Comparison with land-based resources," *Ore Geology Reviews*, vol. 51, pp. 1–14, jun 2013.

[6] J. R. Hein, F. Spinardi, N. Okamoto, K. Mizell, D. Thorburn, and A. Tawake, "Critical metals in manganese nodules from the Cook Islands EEZ, abundances and distributions," *Ore Geology Reviews*, vol. 68, pp. 97–116, jul 2015.

[7] P. Rona, "The changing vision of marine minerals," *Ore Geology Reviews*, vol. 33, no. 3-4, pp. 618–666, jun 2008.

[8] C. Morgan, "Environmental Impacts of Deep-Ocean mining - the importance of Manganese," in *Marine Environmental Pollution, 2, Dumping and Mining*, R. Geyer, Ed. Amsterdam-Oxford-Newyork: Elsevier Scientific Publishing Company, 1981, ch. 14, pp. 415–435.

[9] C. Johnson and J. Otto, "Manganese nodule project economics," *Resources Policy*, vol. 12, no. 1, pp. 17–28, mar 1986.

[10] C. Morgan, N. Odunton, and A. Jones, "Synthesis of Environmental Impacts of Deep Seabed Mining," *Marine Georesources & Geotechnology*, vol. 17, no. Nov, pp. 307–356, 1999.

[11] R. A. Kotlinski, D. Maciag, and D. Zawadzki, "Potential and Recent Problems of the Possible Polymetallic Sources in the Oceanic Deposits," in *Geology and mineral resources of the world's oceans*, 2nd ed. Kiev: Department of Marine Geology and Sedimentary Ore Formation of National Academy of Sciences of Ukraine (Kiev), 2015, pp. 65–80.

[12] ISA, "A geological model of polymetallic nodule deposits in the Clarion-Clipperton Fracture Zone," ISA, Tech. Rep., 2010. [Online]. Available: https://www.isa.org.jm/sites/default/files/files/documents/tstudy6.pdf

[13] R. Healing and A. Archer, "Manganese nodules an example of a Lasky distribution?" *Resources Policy*, vol. 1, no. 6, pp. 306–312, Dec. 1975.

[14] A. Usui, A. Nishimura, M. Tanahashi, and S. Terashima, "Local variability of manganese nodule facies on small abyssal hills of the Central Pacific Basin," *Marine Geology*, vol. 74, no. 3-4, pp. 237–275, feb 1987.

[15] J. Frazer and M. Fisk, "Geological factors related to characteristics of sea-floor manganese nodule deposits," *Deep Sea Research Part A. Oceanographic Research Papers*, vol. 28, no. 12, pp. 1533–1551, Dec. 1981.

[16] R. Sharma, N. Khadge, and S. Jai Sankar, "Assessing the distribution and abundance of seabed minerals from seafloor photographic data in the Central Indian Ocean Basin," *International Journal of Remote Sensing*, vol. 34, no. 5, pp. 1691–1706, mar 2013.

[17] J. Kim, K. Hyeong, H.-B. Lee, and Y.-T. Ko, "Relationship between polymetallic nodule genesis and sediment distribution in the KODOS (Korea Deep Ocean Study) Area, Northeastern Pacific," *Ocean Science Journal*, vol. 47, no. 3, pp. 197–207, sep 2012.

[18] C. Mckenzie, C. Payne, G. Partington, E. Puccioni, C. Wildman, and D. Thorburn, "Predictive modelling of polymetallic nodule deposits in the Cook Island Exclusive Economic Zone," in *AusIMM NZ branch conference*, Dunedin, 2015.

[19] D. S. Cronan, "Controls on the Nature and Distribution of Manganese Nodules in the Western Equatorial Pacific Ocean," in *Marine Minerals: Advances in Research and Resource Assessment*, P. G. Teleki, M. R. Dobson, J. R. Moore, and v. U., Eds. Dordrecht: Springer Netherlands, 1987, pp. 177–188.

[20] C. Morgan, "A geological model of polymetallic nodule deposits in the Clarion-Clipperton Fracture Zone, Subreport of ISA technical brief 6: 22-96," ISA, Tech. Rep. March, 2012.

[21] ISA, "Prospectors Guide for polymetallic nodule deposits in the Clarion-Clipperton fracture zone, Subreport of ISA technical brief 6: 97-211," ISA, Tech. Rep. March, 2010.

[22] J. Schmidhuber, "Deep Learning in neural networks: An overview," *Neural Networks*, vol. 61, pp. 85–117, 2015.

[23] P. Halbach, "Processes controlling the heavy metal distribution in Pacific ferromanganese nodules and crusts," *Geologische Rundschau*, vol. 75, no. 1, pp. 235–247, 1986.

[24] R. A. Kotlinski, "Metallogenesis of the world's ocean against the background of oceanic crust evolution," *Special Papers, Polish Geological Institute*, vol. 4, 1999.

[25] H. W. Menard and J. Frazer, "Manganese nodules on the sea floor: inverse correlation between grade and abundance," *Science*, vol. 199, no. 4332, pp. 969–971, 1978.

[26] General Bathymetric Chart of the Oceans website, "GEBCO 30 arc-second grid." [Online]. Available: http://www.gebco.net/data_and_products/gridded_bathymetry_data/gebco_30_second_grid/

[27] P. Weatherall, K. Marks, M. Jakobsson, T. Schmitt, S. Tani, J. Arndt, M. Rovere, D. Chayes, V. Ferrini, and R. Wigley, "A new digital bathymetric model of the world's oceans," *Earth and Space Science*, vol. 2, no. 8, pp. 331–345, aug 2015. [Online]. Available: http://doi.wiley.com/10.1002/2015EA000107

[28] NOAA National Centers for Environmental Information, "Main page." [Online]. Available: http://www.ngdc.noaa.gov/

[29] R. Warnken, W. Virden, and C. Moore, "The NOAA and MMS Marine Minerals Bibliography (1992)," 1992. [Online]. Available: http://www.ngdc.noaa.gov/docucomp/page?xml=NOAA/NESDIS/NGDC/MGG/Geology/iso/xml/G00497.xml&view=getDataView&header=none

[30] Ocean Drilling Program (2005), "Archive of Core and Site/Hole Data and Photographs from the Ocean Drilling Program (ODP)." [Online]. Available: http://www.ngdc.noaa.gov/docucomp/page?xml=NOAA/NESDIS/NGDC/MGG/Geology/iso/xml/G03298.xml&view=getDataView&header=none

[31] National Ocean Service (2013), "NOAA/NOS and USCGS Seabed Descriptions from Hydrographic Surveys." [Online]. Available: http://www.ngdc.noaa.gov/docucomp/page?xml=NOAA/NESDIS/NGDC/MGG/Geology/iso/xml/G10163.xml&view=getDataView&header=none

[32] Curators of Marine and Lacustrine Geological Samples Consortium, "Index to Marine and Lacustrine Geological Samples (IMLGS)." [Online]. Available: http://www.ngdc.noaa.gov/docucomp/page?xml=NOAA/NESDIS/NGDC/MGG/Geology/iso/xml/G00028.xml&view=getDataView&header=none

[33] Integrated Ocean Drilling Program (2010), "Archive of Core and Site/Hole Data and Photographs from the Integrated Ocean Drilling Program (IODP)." [Online]. Available: http://www.ngdc.noaa.gov/docucomp/page?xml=NOAA/NESDIS/NGDC/MGG/Geology/iso/xml/IntegratedOceanDrillingProgramUSIO.xml&view=getDataView&header=none

[34] Deep Sea Drilling Project (1989), "Archive of Core and Site/Hole Data and Photographs from the Deep Sea Drilling Project (DSDP)." [Online]. Available: http://www.ngdc.noaa.gov/docucomp/page?xml=NOAA/NESDIS/NGDC/MGG/Geology/iso/xml/G00993.xml&view=getDataView&header=none

[35] International Seabed Authority, "Central data repository." [Online]. Available: https://www.isa.org.jm/central-data-repository

[36] Oregon State University Ocean Productivity page, "Ocean Productivity." [Online]. Available: http://www.science.oregonstate.edu/ocean.productivity/index.php

[37] R. A. Koski, C. R. German, and J. R. Hein, "Fate of Hydrothermal Products from Mid ocean Ridge Hydrothermal Systems - Nearfield to Global Perspectives," in *Energy and Mass Transfer in Marine and Hydrothermal Systems*, P. Halbach, V. Tunnicliffe, and J. R. Hein, Eds. Berlin, Germany: Dahlem University Press, 2003, pp. 317–335.

[38] C. Morgan, "Manganese Nodules, Again?" in *Oceans 2011, Kona*. Waikoloa: IEEE, 2011, pp. 1–6.

[39] M. Behrenfeld and P. Falkowski, "Photosynthetic rates derived from satellite-based chlorophyll concentration," *Limnology and Oceanography*, vol. 42, pp. 1–20, 1997.

[40] R. A. Kotlinski, "Relationships Between Nodule Genesis And Topography In The Eastern Area Of The Clarion-Clipperton region," in *Establishment of a geological model of polymetallic nodule deposits in the Clarion-Clipperton fracture zone of the equatorial North Pacific ocean*. Nadi, Fiji: International Seabed Authority, 2009, ch. 12.

[41] K. Mewes, J. M. Mogollón, A. Picard, C. Rühlemann, T. Kuhn, K. Nöthen, and S. Kasten, "Impact of depositional and biogeochemical processes on small scale variations in nodule abundance in the Clarion-Clipperton Fracture Zone," *Deep-Sea Research Part I: Oceanographic Research Papers*, vol. 91, pp. 125–141, 2014.

[42] Y. Ko, S. Lee, J. Kim, K.-H. Kim, and M.-S. Jung, "Relationship between Mn nodule abundance and other geological factors in the northeastern pacific: Application of GIS and probability method," *Ocean Science Journal*, vol. 41, no. 3, pp. 149–161, sep 2006.

[43] M. Behrenfeld and P. Falkowski, "A consumer's guide to phytoplankton primary productivity models," *Limnology and Oceanography*, vol. 42, pp. 1479–1491, 1997.

[44] J. E. Andrews, C. Landmesser, and M. Morgenstein, “Hawaii Institute of Geophysics data banks for Manganese collections and hydration-rind dating,” Hawaii Institute of Geophysics, University of Hawaii, Tech. Rep., 1973.

[45] R/V Moana Wave (Ship), J. E. Andrews, N. S. F. (U.S.), and H. I. of Geophysics, “Ferromanganese deposits of the ocean floor (Cruise report Mn-74-01 R/V Moana Wave),” National Science Foundation, Tech. Rep., 1974.

[46] S. Margolis and C. Bowser, “Ferromanganese deposits of the ocean floor (Cruise report Mn-74-02 R/V Moana Wave),” Hawaii Institute of Geophysics, University of Hawaii, Tech. Rep., 1975.

[47] J. L. Bischoff and D. Z. Piper, Eds., *Marine Geology and Oceanography of the Pacific Manganese Nodule Province*, 1st ed. Boston, MA: Springer US, 1979.

[48] C. Morgan, J. A. Nichols, B. W. Selk, J. R. Toth, and C. Wallin, “Preliminary analysis of exploration data from Pacific deposits of manganese nodules,” *Marine Georesources And Geotechnology*, vol. 11, no. 1, pp. 1–25, 1993.

[49] H.-S. Jung, Y.-T. Ko, S.-B. Chi, and J.-W. Moon, “Characteristics of Seafloor Morphology and Ferromanganese Nodule Occurrence in the Korea Deep-sea Environmental Study (KODES) Area, NE Equatorial Pacific,” *Marine Georesources & Geotechnology*, vol. 19, no. 3, pp. 167–180, jul 2001.

[50] S. H. Lee and K.-H. Kim, “Side-Scan Sonar Characteristics and Manganese Nodule Abundance in the Clarion-Clipperton Fracture Zones, NE Equatorial Pacific,” *Marine Georesources & Geotechnology*, vol. 22, no. 1-2, pp. 103–114, jan 2004.

[51] V. Stoyanova and R. A. Kotlinski, “Distribution particularities of nodules occurrence in the eastern Clarion - Clipperton Zone (NE Pacific),” in *Geosciences 2009*, Sofia, Bulgaria, 2009, pp. 99–100.

[52] M. Bau, K. Schmidt, A. Koschinsky, J. Hein, T. Kuhn, and A. Usui, “Discriminating between different genetic types of marine ferro-manganese crusts and nodules based on rare earth elements and yttrium,” *Chemical Geology*, vol. 381, pp. 1–9, aug 2014.

[53] A. Krizhevsky, I. Sulskever, and G. Hinton, “Imagenet classification with deep convolutional neural networks,” in *Advances in Neural Information Processing Systems 25*, F. Pereira, C. J. C. Burges, L. Bottou, and K. Q. Weinberger, Eds. Curran Associates, Inc., 2012, pp. 1097–1105.

[54] A. Graves, H. B., S. F., M. Liwicki, and J. Schmidhuber, “Unconstrained on-line handwriting recognition with recurrent neural networks,” in *Advances in Neural Information Processing Systems 20*, J. C. Platt, D. Koller, Y. Singer, and S. T. Roweis, Eds. Curran Associates, Inc., 2008, pp. 577–584.

[55] G. Hinton, L. Deng, D. Yu, G. Dahl, A.-R. Mohamed, N. Jaitly, V. Vanhoucke, P. Nguyen, T. Sainath, and B. Kingsbury, “Deep Neural Networks for Acoustic Modeling in Speech Recognition,” *IEEE Signal Processing Magazine*, vol. 29, no. 6, pp. 82–97, 2012.

[56] C. Neocleous and C. Schizas, “Artificial neural network learning: A comparative review,” in *Methods and Applications of Artificial Intelligence*. Springer Berlin Heidelberg, 2002, pp. 300–313.

[57] T. Tieleman and G. Hinton, “Lecture 6.5 - rmsprop, COURSERA: Neural Networks for Machine Learning,” 2012.

[58] L. Deng, G. Hinton, and B. Kingsbury, “New types of deep neural network learning for speech recognition and related applications: an overview,” *2013 IEEE International Conference on Acoustics, Speech and Signal Processing*, pp. 8599–8603, 2013.

[59] D. Stathakis, “How many hidden layers and nodes?” *International Journal of Remote Sensing*, vol. 30, no. 8, pp. 2133–2147, 2009.

[60] M. Zeiler, M. Ranzato, R. Monga, M. Mao, K. Yang, Q. Le, P. Nguyen, A. Senior, V. Vanhoucke, J. Dean, and G. Hinton, “On rectified linear units for speech processing,” *IEEE International Conference on Acoustics, Speech and Signal Processing - Proceedings*, pp. 3517–3521, 2013.

[61] D. Powers, “Evaluation: From Precision, Recall and F-Measure to ROC, Informedness, Markedness & Correlation,” *Journal of Machine Learning Technologies*, vol. 2, no. 1, pp. 37 – 63, 2011.

[62] N. Srivastava, G. Hinton, A. Krizhevsky, I. Sutskever, and R. Salakhutdinov, “Dropout : A Simple Way to Prevent Neural Networks from Overfitting,” *Journal of Machine Learning Research (JMLR)*, vol. 15, pp. 1929–1958, 2014.

[63] N. Cressie, “The origins of kriging,” *Mathematical Geology*, vol. 22, no. 3, pp. 239–252, apr 1990.

[64] G. Matheron, “Principles of geostatistics,” *Economic Geology*, vol. 58, no. 8, pp. 1246–1266, dec 1963.

[65] P. Dumitru, M. Plopeanu, and D. Badea, “Comparative study regarding the methods of interpolation,” *Recent Advanced in Geodesy and Geomatics EngineeringConference Proceedings*, pp. 45–52, 2013.

[66] S. Lee and N. T. Dan, “Probabilistic landslide susceptibility mapping in the Lai Chau province of Vietnam: focus on the relationship between tectonic fractures and landslides,” *Environmental Geology*, vol. 48, no. 6, pp. 778–787, 2005.

[67] I. Yilmaz, “Landslide susceptibility mapping using frequency ratio, logistic regression, artificial neural networks and their comparison: A case study from Kat landslides (Tokat-Turkey),” *Computers and Geosciences*, vol. 35, no. 6, pp. 1125–1138, 2009.